Electronic Supplementary Material (ESI) for Materials Horizons.

Supplementary Information

Exploring the Mpemba Effect: A Universal Ice Pressing Enables Porous Ceramics

Authors

Xiaodan Yang‡ [ab], Yao Shan‡ [ab], Ying Hong‡ [ab], Zhuomin Zhang [ab], Shiyuan Liu [ab], Xiaodong Yan [ab], Xuetian Gong[c], Guangzu Zhang [c], Zhengbao Yang[a*]

Affiliations

a. Department of Mechanical and Aerospace Engineering, Hong Kong University of Science and Technology, Clear Water Bay, Hong Kong, China. E-mail: zbyang@ust.hk
b. Department of Mechanical Engineering, City University of Hong Kong, Hong Kong, China
c. School of Optical and Electronic Information, Engineering Research Center for Functional Ceramic MOE and Wuhan National Laboratory for Optoelectronics, Huazhong University of Science and Technology, Wuhan 430074, China

‡ These authors are co-first authors in this work.

This PDF file includes:

Other Supplementary Materials for this manuscript include the following:

Movies S1

Supplementary Text

Materials and Methods

Preparation of the PZT green bodies

The polyvinyl alcohol (PVA) solution (Alfa Aesar, medium molecular weight) 4% by weight of powders was mixed with the purchased Pb $(Zr_{0.52}Ti_{0.48})O_3$ (PZT) powders (Suzhou PANT Technology Co., Ltd.). Then, the powders were put into a steel mold and compressed gently to form a cylinder green body with a diameter of 90 mm and a height of 2 mm. Steel molds (cuboid, cylindrical, etc.) were also used to prepare ceramics in different shapes.

Preparation of the BTO pellets

To prepare the Barium titanate (BTO) green body, PVA binder (4% solution) was mixed with the purchased powders (Macklin, 1μm). Then, the powders were shaped into a cylinder green body with a diameter of 90 mm and a height of 2 mm in a steel mold. Afterward, green bodies are packed in a plastic bag and put into a sealed container filled with water. The container is submerged in liquid nitrogen and directly frozen for 5 min. Afterward, it was removed from the liquid nitrogen until the ice fully melted at room temperature. Finally, the green compacts are sintered at 1350°C for two hours after debinder at 600 °C for two hours.

Setup of ice pressing process

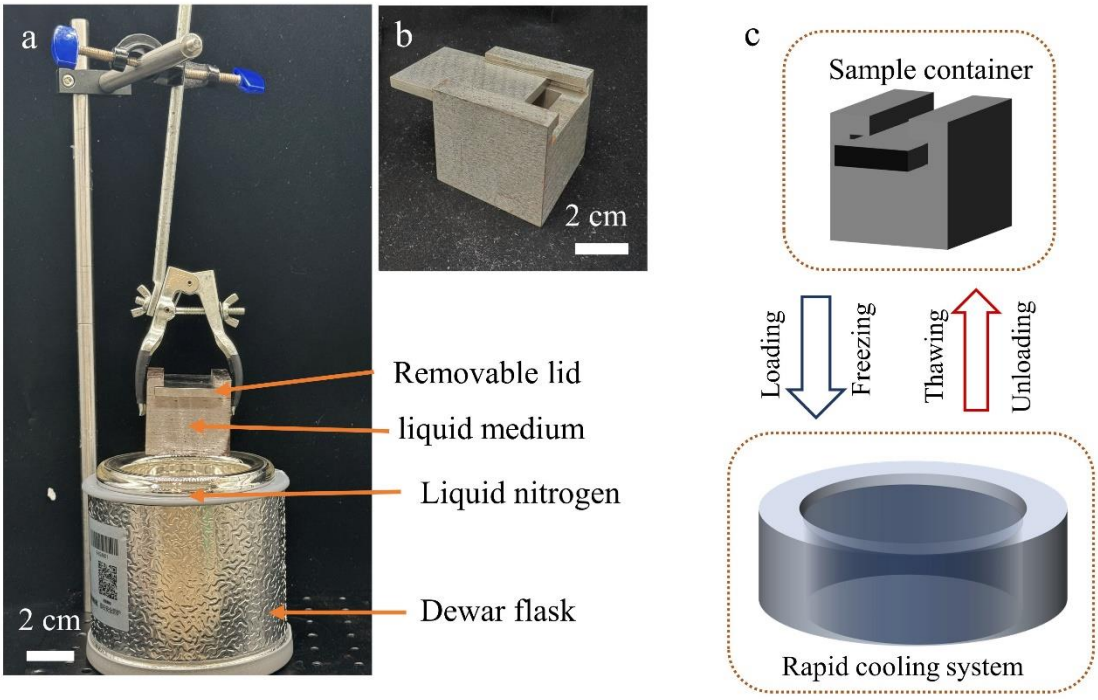

Fig. S1 Setup of ice pressing method. (a) A photograph of the ice pressing device, involves a rapid cooling system and a sample container with a liquid medium. (b) Details of the sample container with a removable lid and liquid medium. (c) Schematic of the ice pressing process. A shaped precursor is put into a closed container with a liquid medium. Afterward, the container is immersed in the cooling system, and the liquid medium transforms into a solid with a specific volume expansion, corresponding to the loading of force on the sample. On the contrary, removing the container from the cooling system corresponds to force unloading.

Observation of the water freezing

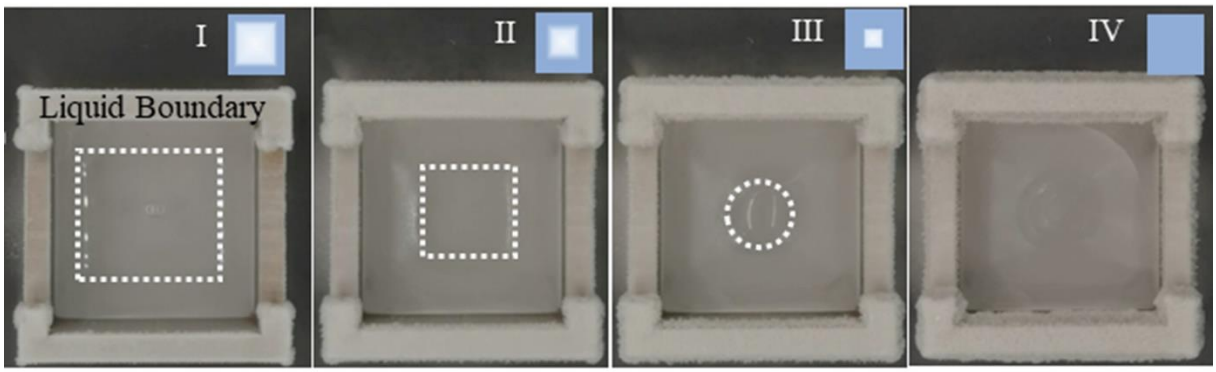

Fig. S2 The digital photograph and the infrared thermal images were taken from the top side of setup to record the temperature. I to IV demonstrate the frozen direction.

Setup and Measurement of ice pressing pressure

The main element is a steel vessel with a removable lid that locks it with certain pressure from a tablet press. When the water turns into ice, the force generated by the expansion of the ice will push the lid, so the pressure is obtained indirectly by measuring the force on the cover. The graph shows the power generated by the freezing process, and it can be divided into five stages (I-IV). The medium is in a liquid state during the I stage, while it is a pseudo-solid state (ice-water mixture) during II-III, and the IV-V stages are in a solid form (ice). The device was preloaded at the beginning of the test (43 MPa). Therefore, the initial pressure is not 0 (stage I). Afterward, liquid nitrogen was poured into the container, and the system started to cool down. In the II stage, there is a noticeable drop in pressure due to the cooling of the equipment. The III stage is a pseudo-solid state, corresponding to water freezing until it freezes into ice when the volume is the largest. If the system (ice) keeps cooling down (IV stage), the ice volume decreases, as well as the force it creates. Finally, once stop adding liquid nitrogen, the ice starts to thaw and upload slowly. To avoid unnecessary energy loss during stage IV, we can control the process by stopping cooling as soon as the water is completely frozen. The medium of ice pressure is not limited to water, it can also be a mixture of other liquid medium and water. Considering the volume change is the key factor to generate high pressure, to obtain a larger pressure range, water is the best medium.

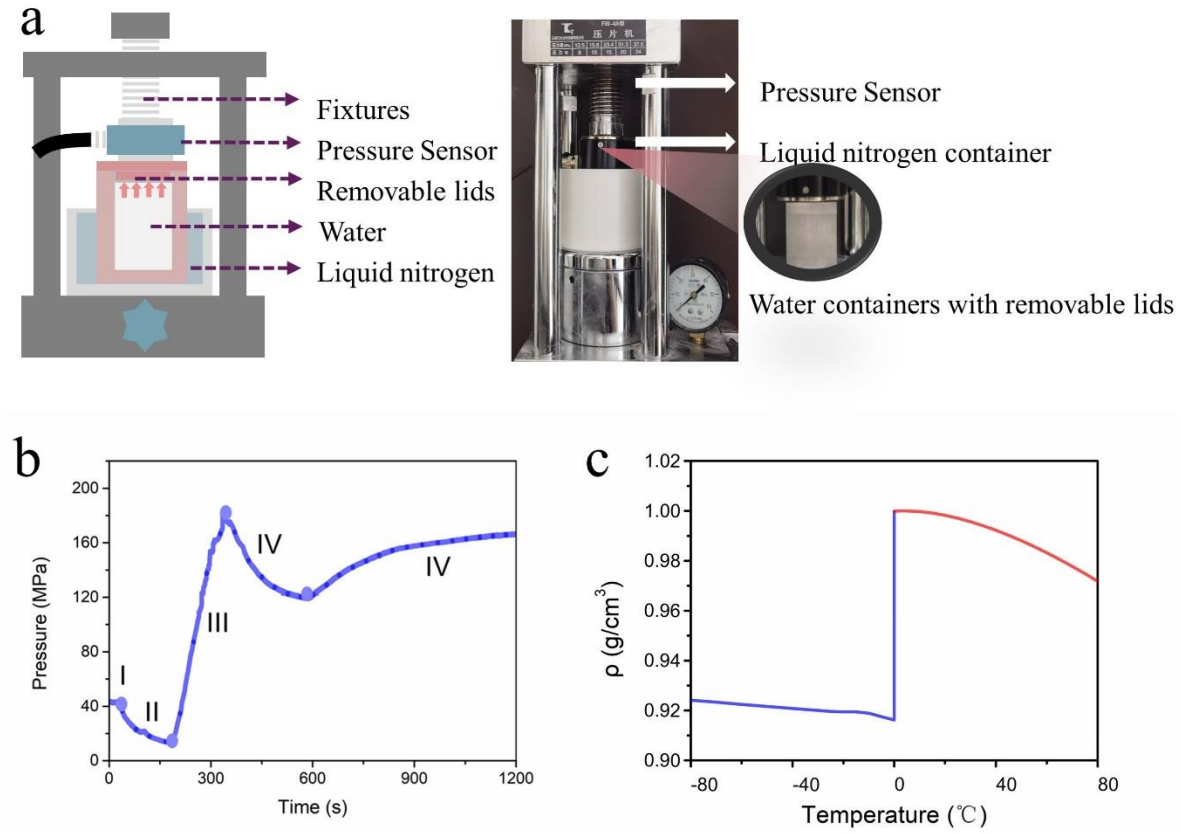

Fig. S3 (a) Photograph of pressure measurement setup of ice pressing method. (b) The force generated by the freezing process. (c) The density of water/ ice at different temperatures.

Observation of the ice crystals via rapid freezing

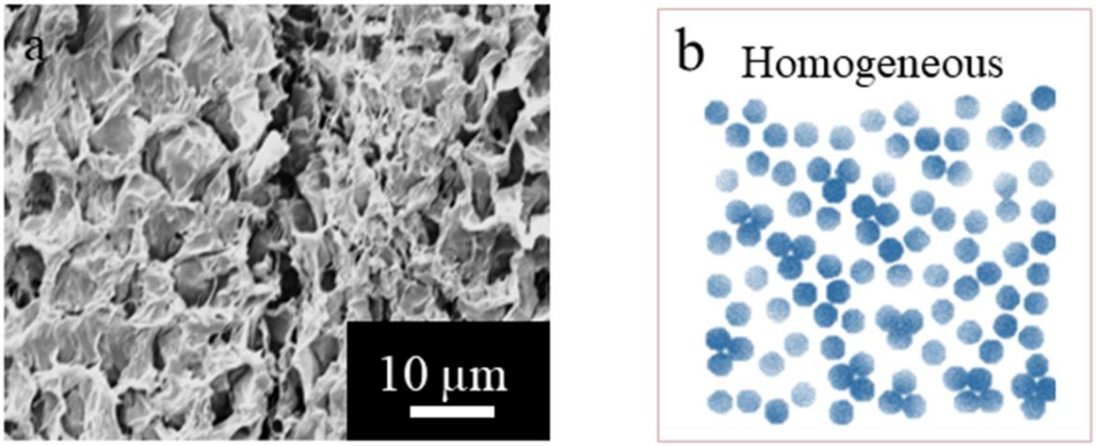

Fig. S4 (a) SEM images of sodium alginate framework after rapid freezing. (b) Schematic of the ice crystals generated by rapid freezing.

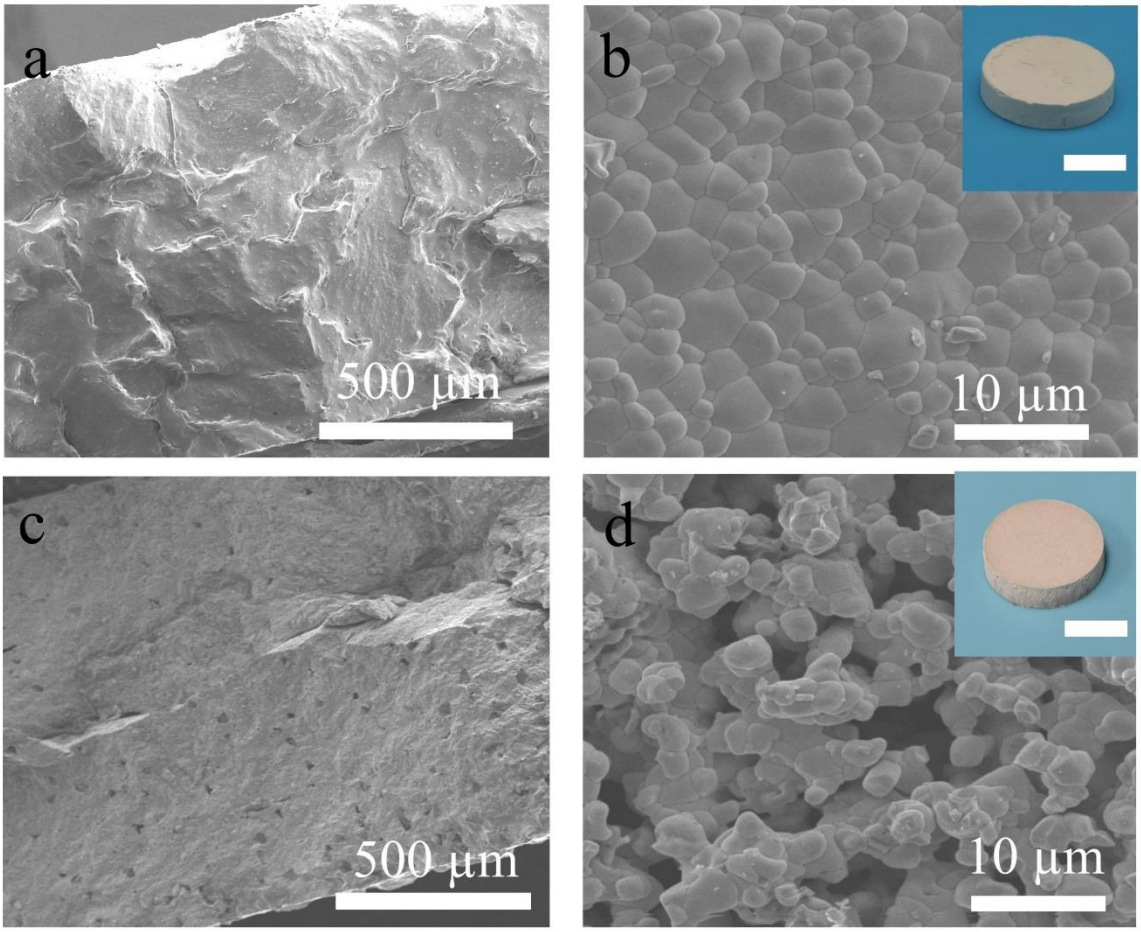

Fig. S5 The SEM images of ICEP-PZT (a-b) and UP-PZT (c-d) pellets. Digital photographs of green body of ICEP-PZT and UP-PZT (Insert, the scale bar is 1 cm).

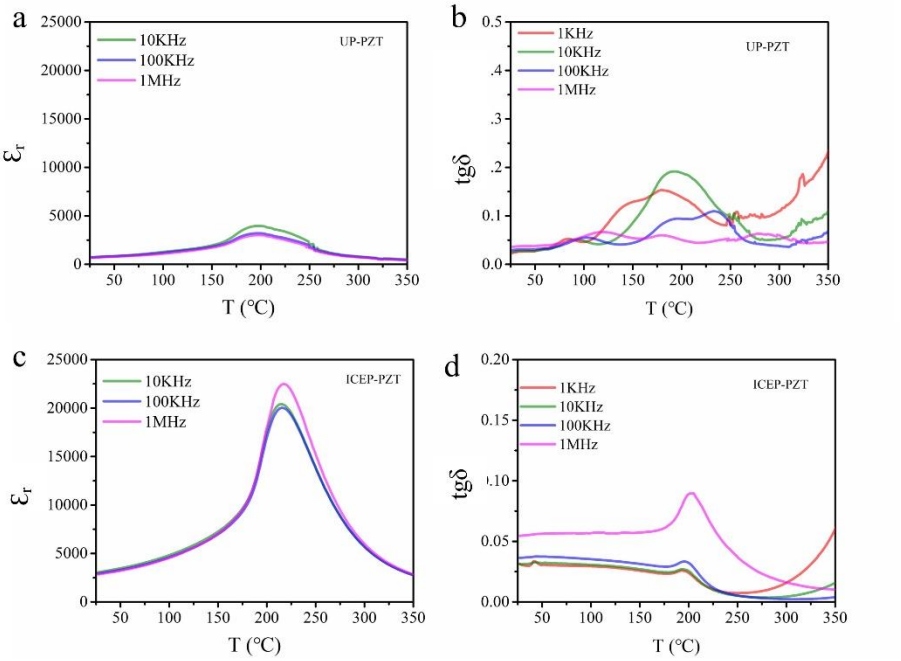

Fig. S6 Comparison of the dielectric properties of PZT ceramics: (a) dielectric constant and (b) dielectric loss.

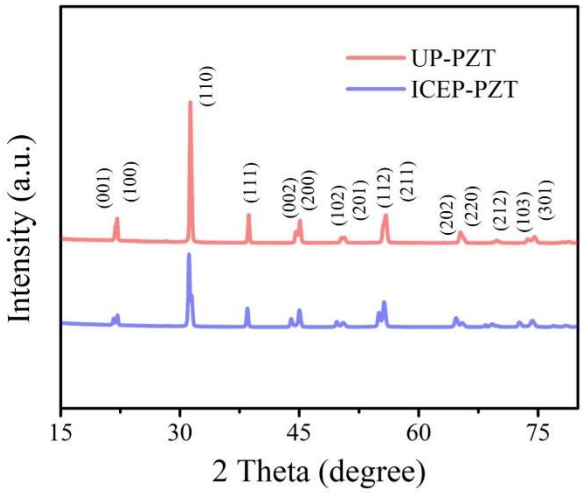

Fig. S7 The XRD patterns of the obtained curved and flat PZT ceramic. The two specimens exhibit an identical crystal structure.

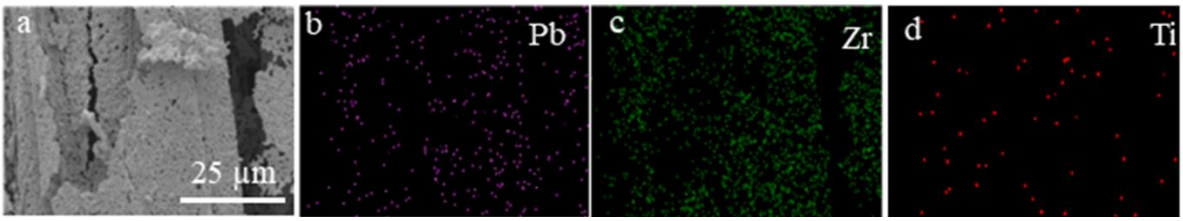

Fig. S8 (a) SEM image and (b-d) Energy dispersive spectroscopy (EDS) mapping of the UP-PZT ceramic framework.

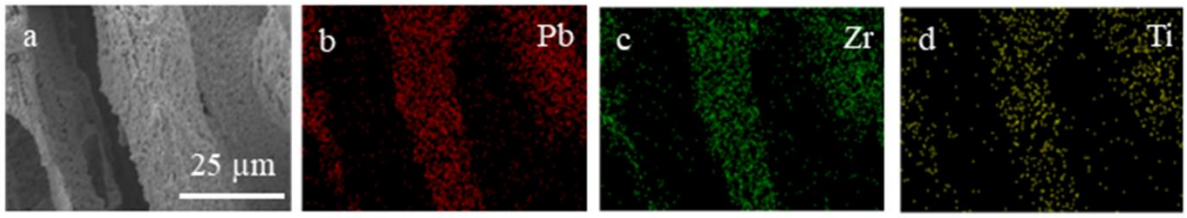

Fig. S9 (a) SEM image and (b-d) Energy dispersive spectroscopy (EDS) mapping of the ICEP-PZT ceramic framewor

Evolution of water freezing phase interface in porous PZT

When applying ice pressing, the frozen interface produces a curved surface instead of a plane. Only when the freezing surface temperature drop lower than the critical temperature, that is, the radius of curvature of the ice-water interface is smaller than the pore radius, the ice interface moves into the pore[1,2]. The behavior of freezing porous materials can be essentially described by the thermodynamic equilibrium and themechanical equilibrium.

Thermodynamic equilibrium of a water-ice system requires the equality of the chemical potential of both phases. It can be described by the Clausius-Clapeyron equation[3]:

$$P_{ice} - P_{water} = \frac{\rho_{water}\Delta H_f}{T_{pore} - T_{bulk}} (1)$$

Where ΔH_f is the enthalpy of melting (334.88 kJ/kg), T_{pore} is the freezing temperature of water in the pore, and T_{bulk} is the freezing temperature of water in ice-water interface. Equation S1 reveals that the temperature gradient during the freezing process will affect the pressure difference on the frozen surface.

Themechanical equilibrium of the water-ice system is governed by the capillary theory. At the capillary scale, the phase interface undergoes a crescent-shaped curvature due to a pressure difference governed by the Young-Laplace equation[4]:

$$\Delta P = \frac{2\gamma_{ice-water}}{R_{pore}} (2)$$

Where ΔP is the Laplace pressure, which is the pressure difference across the fluid interface ($P_{ice} - P_{water}$), $\gamma_{ice\text{-}water}$ is the surface energy between ice and water (33×10^{-3} N/m), and r is the curve radius of the ice-water phase interface.

Combining equations (1) and (2) yields the relationship between the freezing temperature and the mean curvature radius, which is as known as the Gibbs-Thomson equation[5,6]:

$$T_{pore} = T_{bulk}\left(1 - \frac{2\gamma_{ice-water}}{\rho_{water}\Delta H_f R_{pore}}\right) (3)$$

Where γ_{iw} is the surface energy between ice and water, ρ_{water} is the density of water, ΔH_f is the enthalpy of freezing, and R_{pore} is the pore radius.

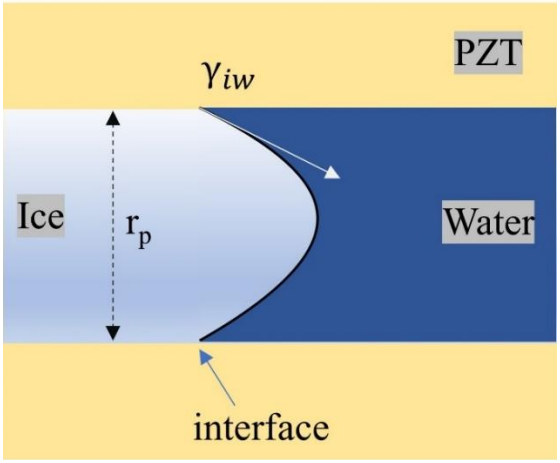

Fig. S10 Schematic of evolution mechanism of water freezing phase interface in porous PZT at the microscale.

Table S1. The comparison of the piezoelectric and dielectric properties between this work and other previous reports.

Samples	Compressing Method	Forming pressure	Density (g/cm^3)	Dielectric constant (RT)	Dielectric Loss (RT)	Remanent polarization ($\mu C/cm^2$)	d_{33} (pC/N)	Ref.
PZT	Uniaxial press	N/A	7.25	1300	N/A	N/A	270	7
PZN–PZT	Uniaxial press	100 MPa	N/A	1232	0.03	37.9	347	8
PZT	Uniaxial press	N/A	7.70	1809	0.02	N/A	505	9
PZT	Uniaxial press	N/A	7.54	957.75	0.005	15.1	225	10
PZT-PNT	Cold isostatic pressing	100 MPa	N/A	N/A	N/A	12	125	11
PZT	Cold isostatic pressing	200 MPa	7.4	1120	0.06	N/A	129	12
PLZT	Cold isostatic pressing	200 MPa	7.6	1269	0.05	N/A	372	12
PZT (57/43)	Cold isostatic pressing	230 MPa	N/A	N/A	N/A	N/A	200	13
UP-PZT	None	N/A	5.80±0.21	773	0.07	32.12	125±11	This work
ICEP-PZT	**Ice pressing**	**180 MPa**	**7.35±0.14**	**3221**	**0.03**	**44.07**	**531±18**	**This work**

Movie S1.

Comparison of in-situ temperature mapping of water (60℃ and 22 ℃)

References

1 O. Coussy and T. Fen-Chong, *Comptes Rendus Mecanique*, 2005, **333**, 507–512.
2 M. Zhou and G. Meschke, in *COUPLED IV: proceedings of the IV International Conference on Computational Methods for Coupled Problems in Science and Engineering*, CIMNE, 2011, pp. 1083–1094.
3 G. Løvoll, Y. Méheust, K. J. Måløy, E. Aker and J. Schmittbuhl, *Energy*, 2005, **30**, 861–872.
4 E Clement, C Baudet, E Guyon and J P Hulin, *J Phys D Appl Phys*, 1987, **20**, 608.
5 J. Zhou and C. Wei, *Cold Reg Sci Technol*, 2020, **171**, 102964.
6 P. Buffat and J. P. Borel, *Phys Rev A (Coll Park)*, 1976, **13**, 2287–2298.
7 L. B. Kong and J. Ma, *Mater Lett*, 2001, **51**, 95–100.
8 J. Du, C. Yang, Y. Li, J. Yan, L. Qiu, L. Wang and K. Zhu, *J. Mater. Sci. Mater. El.*, 2023, **34**, 780.
9 A. Benčan, B. Malič, S. Drnovšek, J. Tellier, T. Rojac, J. Pavlič, M. Kosec, K. G. Webber, J. Rödel and D. Damjanovič, *J. Am. Ceram. Soc.*, 2012, **95**, 651–657.
10 Thongsanitgarn P, Watcharapasorn A and Jiansirisomboon S., *Surf. Rev. Lett.*, 2010, **17**, 1–7.
11 E. Mensur-Alkoy, M. Y. Kaya, D. Avdan and S. Alkoy, *IEEE Trans Ultrason Ferroelectr Freq Control*, 2016, **63**, 907–914.
12 M. Siddiqui, J. J. Mohamed and Z. A. Ahmad, *J. Aust. Ceram. Soc.*, 2020, **56**, 371–377.
13 M. A. Zaghete, J. A. Varela, M. Cilense, C. O. Paiva-Santos, W. C. Las and E. Longo, *Ceram. Int.*, 1999, **25**, 239–244.